jmb Article

Structural and Biochemical Characterization of the Interaction between LGN and Frmpd1

Zhu Pan[1,2], Yuan Shang[3], Min Jia[1,2], Lu Zhang[1,2], Caihao Xia[1,2], Mingjie Zhang[3,4], Wenning Wang[1,2] and Wenyu Wen[1,2]

*1 - **Key Laboratory of Molecular Medicine,** Ministry of Education, Department of Biochemistry and Molecular Biology, and Institutes of Biomedical Sciences, Shanghai Medical College, Fudan University, Shanghai 200032, P. R. China*
*2 - **Department of Chemistry,** Shanghai Key Laboratory of Molecular Catalysis and Innovative Materials, Fudan University, Shanghai 200433, P. R. China*
*3 - **Division of Life Science,** State Key Laboratory of Molecular Neuroscience, Hong Kong University of Science and Technology, Kowloon, Hong Kong, P. R. China*
*4 - **Center of Systems Biology and Human Health,** School of Science and Institute for Advanced Study, Hong Kong University of Science and Technology, Kowloon, Hong Kong, P. R. China*

***Correspondence to Wenning Wang and Wenyu Wen:** W. Wang is to be contacted at Department of Chemistry, Fudan University, 220 Handan Road, Shanghai 200433, P. R. China; W. Wen, Institutes of Biomedical Sciences, Shanghai Medical College, Fudan University, 131 Dong An Road, Shanghai 200032, P. R. China. wnwang@fudan.edu.cn; wywen@fudan.edu.cn*
http://dx.doi.org/10.1016/j.jmb.2013.01.003
Edited by R. Huber

Abstract

The tetratricopeptide repeat (TPR) motif-containing protein LGN binds multiple targets and regulates their subcellular localizations and functions during both asymmetric and symmetric cell divisions. Here, we characterized the interaction between LGN-TPR motifs and FERM and PDZ domain containing 1 (Frmpd1) and reported the crystal structure of the complex at 2.4 Å resolution. A highly conserved fragment at the center of Frmpd1 of ~20 residues was found to be necessary and sufficient to bind to LGN-TPR. This Frmpd1 fragment forms an extended structure and runs along the concave channel of the TPR superhelix in an antiparallel manner in the complex. Structural comparisons and biochemical studies of LGN/Frmpd1 and other known LGN/target interactions demonstrate that the LGN-TPR motifs are versatile and capable of recognizing multiple targets via diverse binding modes. Nevertheless, a conserved "E/QxEx$_{4-5}$E/D/Qx$_{1-2}$K/R" motif in LGN/Pins (*p*artner of *ins*cuteable) TPR binding proteins has been identified.

Introduction

A fundamental mechanism for cellular differentiation and self-renewal in invertebrate and vertebrate development is asymmetric cell division, which requires precise orientations of mitotic spindles along intrinsic or extrinsic polarity axes.[1–5] In *Drosophila* neuroblasts, a key regulator of cell polarity and spindle orientation is Pins (*p*artner of *ins*cuteable; LGN/AGS3 in mammals), which plays roles in several crucial pathways such as the Par3/Insc (*insc*uteable; mInsc in mammals)/Pins/Gαi and the Pins/Mud (*mu*shroom body *d*efect; NuMA in mammals)/dynein pathways.[6–11] Pins/LGN consist of eight tetratricopeptide repeat (TPR) motifs in their N-terminal half[12–14] and three or four GoLoco motifs (also referred to as G-protein regulatory or GPR motifs) in the C-terminal half. Both the TPR and the GoLoco motifs are implicated in protein–protein interactions.[15,16] Each GoLoco motif of Pins/LGN is capable of binding to GDP-bound Gαi,[7,17,18] and this interaction is responsible for stable cortical localization of Pins/LGN.[19] The TPR motifs of Pins/LGN have multiple binding partners. Pins/LGN localize at the apical cortex with the Par complex by binding to Insc/mInsc via their eight TPR

motifs.[6,12,20,21] This apical localized Pins/LGN recruits Mud/NuMA to regulate the mitotic spindle orientation.[8–10,22]

The canonical TPR motif is a 34-amino-acid protein–protein interaction module found in multiple copies in a wide range of proteins with diverse functions such as cell cycle regulations, gene transcription and splicing processes, protein trafficking, and protein folding.[16,23] Each TPR motif adopts a helix–turn–helix fold, and multiple TPR motifs often form a right-handed superhelical structure with a continuous amphipathic groove suitable for the recognition of target proteins. The molecular mechanisms governing the formations of the TPR-mediated LGN/mInsc, Pins/Insc, and LGN/NuMA complexes have been recently elucidated.[12–14] The TPR motifs of LGN/Pins have distinct structural features compared to those in canonical TPR motifs. The αA and αB helices of LGN/Pins TPRs are longer (40 amino acids per TPR) than the corresponding helices in the canonical TPR motifs, and the packing geometry is also different. Although the extended helix was also observed in other TPR proteins before,[24,25] it is first reported in LGN/Pins that these longer helices were found to appear regularly in tandem repeats.[12–14] In the complexes, the LGN/Pins binding fragments of mInsc/Insc and NuMA form elongated structures and bind to the concave channel formed by the TPR motifs. Specifically, the NuMA fragment adopts an extended conformation, whereas the mInsc/Insc fragments form a short α-helix followed by an extended region. It is noted that the LGN/Pins TPR-binding regions of NuMA and mInsc/Insc share very low sequence identity, implying that LGN/Pins TPR motifs are structurally versatile in binding to diverse target proteins.

FERM and PDZ domain containing 1 (Frmpd1) was first reported as a regulatory binding partner of AGS3, and the binding sites between AGS3 and Frmpd1 were mapped to the eight TPR motifs of AGS3 and a short fragment of Frmpd1 (amino acids 901–938).[26] Another recent study has demonstrated that Frmpd1 is also a LGN-TPR binder, and a 50-residue fragment (amino acids 901–951) of Frmpd1 was suggested to bind to LGN following a similar mode as mInsc does.[14] As the TPR motifs of AGS3 and LGN are highly similar (77% sequence identity), we assume that they bind to Frmpd1 with a more or

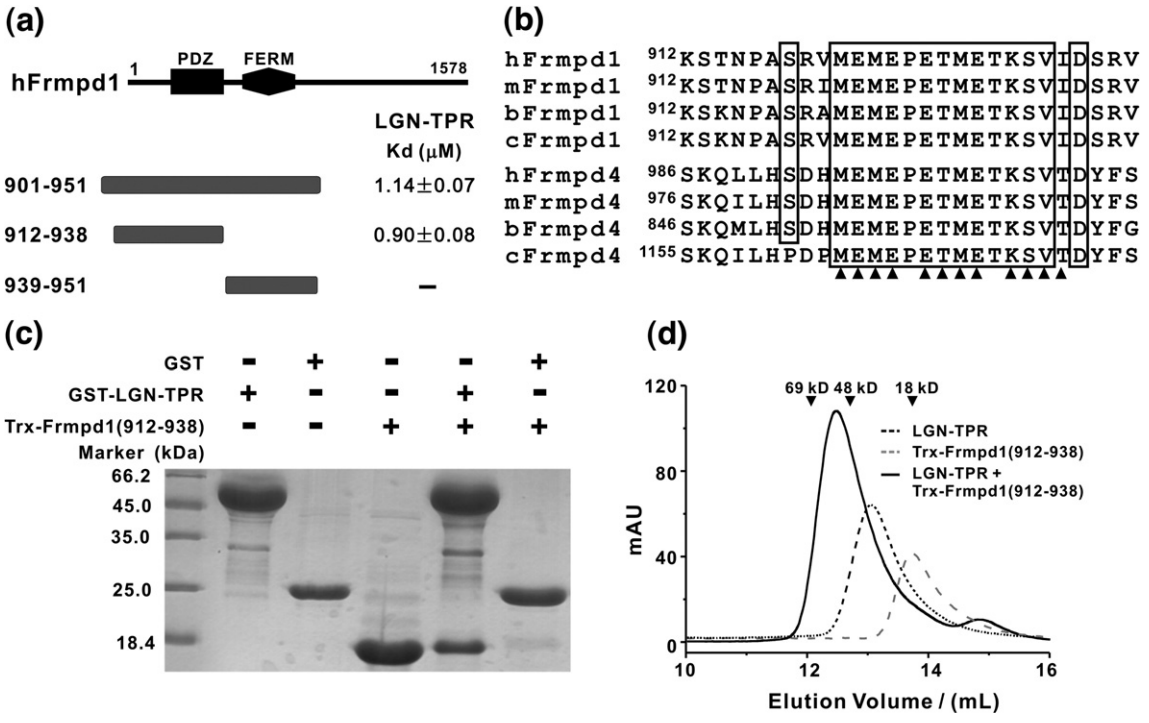

Fig. 1. Characterization of the interaction between LGN and Frmpd1. (a) ITC-based measurements of the bindings between various Frmpd1 fragments and LGN-TPR. (b) Sequence alignment of the Frmpd1 and Frmpd4 fragments showing that the residues involved in contacting with LGN are highly conserved. h, *Homo sapiens*; m, *Mus musculus*; b, *Bos taurus*; c, *Canis lupus familiaris*. In the alignment, the absolutely conserved amino acids are highlighted with box. The residues involved in the LGN interaction are indicated with triangles. (c) GST fusion protein-based pull-down assay showing that GST-LGN-TPR robustly binds to Trx-Frmpd1(912–938). (d) Analytical gel-filtration analysis showing that LGN-TPR and Trx-Frmpd1(912–938) formed a 1:1 stoichiometric complex. The elution volumes of the molecular mass standards are indicated at the top of the panel.

less same mechanism. However, the structural basis underlying the interaction between Frmpd1 and LGN/AGS3 is not clear. In this work, we characterized the interaction between LGN-TPR and Frmpd1 in detail. The high-resolution crystal structure of the LGN/Frmpd1 complex solved in this work reveals that LGN binds to Frmpd1 following a mechanism similar to that of NuMA but distinct from that of mInsc. Structural comparison of known LGN/Pins TPR/target complexes reveals the presence of a conserved "E/QxEx$_{4-5}$E/D/Qx$_{1-2}$K/R" motif in LGN/Pins TPR binding proteins. Further competition experiments demonstrate that NuMA and Frmpd1 compete with each other in binding to LGN, whereas mInsc can efficiently block the associations of both Frmpd1 and NuMA with LGN.

Results

The interaction between LGN and Frmpd1

We first confirmed the LGN/Frmpd1 interaction by showing that the mouse LGN-TPR motifs (TPR0-7, amino acids 15–350)[12] bind to a human Frmpd1 fragment (amino acids 901–951)[14] with a $K_d \sim 1$ μM (Fig. 1a). Sequence alignment of Frmpd1 and its group members from different species pointed to the presence of a highly conserved, short peptide fragment (amino acids 912–938) within the TPR binding site (Fig. 1b),[12,14] indicating that this fragment may be responsible for TPR binding. Glutathione *S*-transferase (GST) pull-down and isothermal titration calorimetry (ITC)-based assays showed that Frmpd1(912–938) robustly binds to LGN-TPR with a comparable affinity as that of the longer Frmpd1(901–951) fragment ($K_d \sim 0.9$ μM; Fig. 1c and d), and deletion of this fragment completely disrupted binding between LGN-TPR and Frmpd1 (Fig. 1a), demonstrating that this 27-residue fragment of Frmpd1 is the minimal binding site for LGN-TPR. We further showed that LGN-TPR and Frmpd1(912–938) form a stable 1:1 stoichiometric complex using analytical gel-filtration chromatography (Fig. 1d). Amino acid sequence analysis reveals that this TPR-binding fragment is also present in Frmpd4 but not in Frmpd2 or Frmpd3 (Fig. 1b).

Crystal structure of the LGN and Frmpd1 complex

To understand the molecular mechanism underlying the LGN/Frmpd1 interaction, we solved the crystal structure of the LGN-TPR/Frmpd1 (amino acids 912–938) complex at 2.4 Å resolution (Table 1). The structure of LGN-TPR in LGN/Frmpd1 complex is composed of sixteen α-helices arranged into eight sequential helix–turn–helix repeats (Fig. 2a and b). The entire length of LGN-TPR is well resolved except for the eleven residues in the loop connecting the αA and αB of TPR3 (amino acids 153–163) and the six residues at the C terminus (amino acids 345–350). Most of the residues of the Frmpd1 fragment are also clearly defined except for the N-terminal eight residues (amino acids 912–919) and the last two residues at the C terminus (amino acids 937–938). The Frmpd1 fragment adopts an extended conformation antiparallel occupying most of the concave channel formed by the eight TPR motifs (Fig. 2a and b), burying a total of 2541 Å^2 surface area (Fig. 2c).

The LGN/Frmpd1 interface can be divided into two regions based on the organization of the TPR superhelix (Fig. 3a and b): (i) TPR0-3 and the C-terminal half of the Frmpd1 fragment and (ii) TPR4-5 and the N-terminal half of the Frmpd1 fragment. The binding of LGN to Frmpd1 is mainly mediated by an extensive polar interaction network. In the region (i), the side chains of Glu926$_{Frmpd1}$ and Glu929$_{Frmpd1}$ form salt bridges with Lys106$_{LGN}$ from α2A and Arg136$_{LGN}$ from α3A, respectively. The side chains

Table 1. Crystallographic data and refinement statistics

Data collection	
Source	SSRF BL17U
Space group	$P6_122$
Unit cell parameters (Å)	$a=b=93.835$, $c=172.863$
Resolution range (Å)	50.00–2.40 (2.44–2.4)
Number of unique reflections	18,332 (861)
Redundancy	13.9 (14.5)
I/σ	31 (3.9)
Completeness (%)	100.0 (100.0)
R_{merge} (%)[a]	10.3 (77.4)
Structure refinement	
Resolution (Å)	41.2–2.40 (2.53–2.40)
R_{cryst}[b]/R_{free}[c] (%)	19.0 (20.4)/23.2 (27.4)
rmsd bounds (Å)/angles (°)	0.0040/0.71
Number of reflections	
Working set	17,319
Test set	930
Protein atoms/water/other atoms	2585/84/63
Average *B*-factor[d]/fragment	
Main chain	56.7/58.5
Side chain	60.3/61.2
Ramachandran plot (%)	
Most favored regions	99.1
Additionally allowed	0.9
Generously allowed	0

Numbers in parentheses represent the value for the highest-resolution shell.

[a] R_{merge} = SUM(ABS($I-\langle I\rangle$))/SUM(I), where I is the intensity of measured reflection and $\langle I\rangle$ is the mean intensity of all symmetry-related reflections.

[b] $R_{cryst} = \sum |F_{calc} - F_{obs}| / \sum F_{obs}$, where F_{obs} and F_{calc} are observed and calculated structure factors, respectively.

[c] $R_{free} = \sum_T |F_{calc} - F_{obs}| / \sum F_{obs}$, where T is a test data set of about 5% of the total unique reflections randomly chosen and set aside prior to refinement.

[d] Refinement is processed with Phenix.refinement, and *B*-factors are extracted by Phenix validation tools.

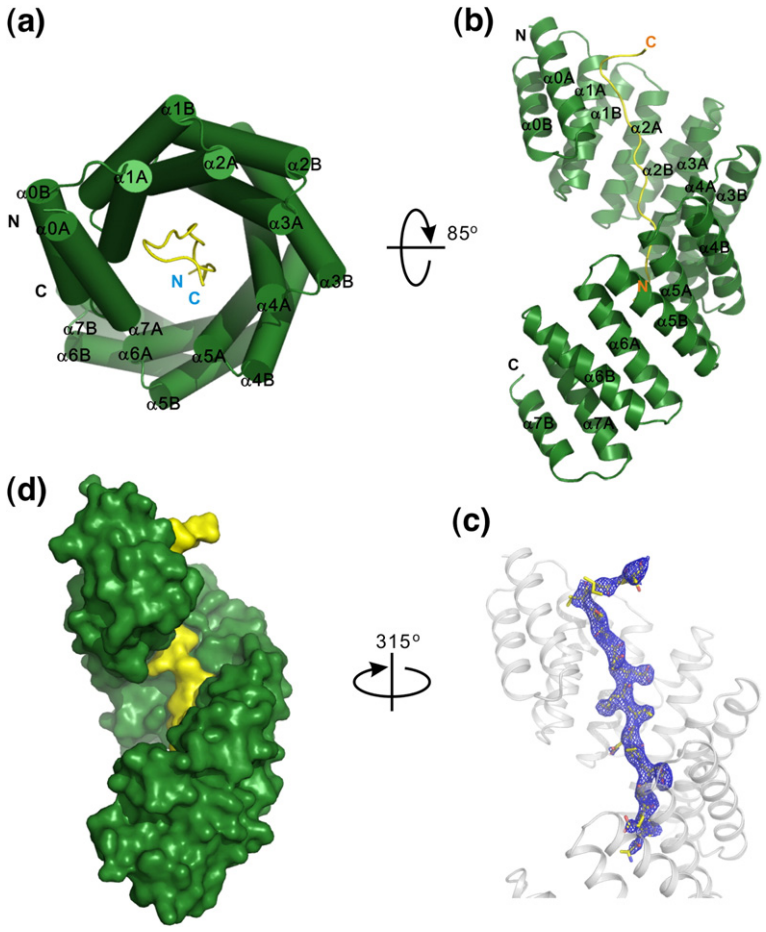

Fig. 2. Overall structure of the LGN/Frmpd1 complex. (a) Cylinder representation of the LGN (green)/Frmpd1 (yellow) complex structure viewed from the top. (b) Ribbon diagram representation of the LGN/Frmpd1 complex viewed from the side. (c) Close-up view of LGN/Frmpd1 complex. The LGN (gray) is shown in ribbon diagram and the Frmpd1 fragment (yellow) is shown in a stick-and-ball model. The F_{obs} – F_{calc} omit map for the Frmpd1 fragment is drawn in blue and contoured at 3.0 σ. (d) Surface presentations of the LGN/Frmpd1 complex with their orientations corresponding to that shown in (c).

of $Thr927_{Frmpd1}$ and $Ser932_{Frmpd1}$ form hydrogen bonds with $Asn140_{LGN}$ from α3A and $Glu25_{LGN}$ from α0A, respectively, while the backbone amide nitrogens or carbonyl oxygens of the C-terminal half of the Frmpd1 fragment (from Thr927 to Val933) form hydrogen bonding interactions with the side chains of Glu25, Gln60, Asn63, Lys96, Asn100, Asn103, and Arg136 from LGN, respectively. The side chain of $Lys931_{Frmpd1}$ forms salt bridges and hydrogen bonds with $Asp81_{LGN}$ from α1B, $Ser55_{LGN}$ from α1A, and the backbone carbonyl oxygen of $Gly93_{LGN}$ from α2A, respectively. Hydrophobic interactions between two residues from Frmpd1 (Val933 and Ile934) and three residues from LGN (Leu18, Leu22 from α0A, and Ile57 from α1A) also contribute to the LGN/Frmpd1 interaction (Fig. 3a). In the region (ii), the backbone carbonyl oxygen of $Pro925_{Frmpd1}$ forms a hydrogen bond with the side chain of $Tyr139_{LGN}$ from α3B. The side chain of $Glu924_{Frmpd1}$ forms salt bridges with $Arg221_{LGN}$ from α4B and $Arg236_{LGN}$ from α5A of LGN, and the backbone amide and carbonyl oxygen of $Glu924_{Frmpd1}$ forms two hydrogen bonds with N^{δ} and O^{δ} of $Asn200_{LGN}$ from α4A. The side chain of $Glu922_{Frmpd1}$ forms a salt bridge with $Arg235_{LGN}$ from α5A and a hydrogen bond with $Gln276_{LGN}$ from α5B, and the backbone amide and carbonyl oxygen of $Glu922_{Frmpd1}$ forms hydrogen bonds with N^{δ} and O^{δ} of $Asn240_{LGN}$ from α5A and $Asn203N^{\delta}$ from α4A. There is a hydrophobic interaction core formed at this region as well, including two residues from Frmpd1 (Met921 and Met923), two residues from α3A (His146 and Lys150), and two residues from α4A (Tyr206 and Leu207) of LGN (Fig. 3b). We performed a series of mutagenesis studies to validate the interactions observed in the LGN-TPR/Frmpd1 complex structure. Disruption of the hydrogen bonds or the salt bridge networks in the LGN/Frmpd1 interface led to decreased or even abolished binding between LGN-TPR and Frmpd1(912–938) (Fig. 3c and d). For example, both substitution of $E924_{Frmpd1}$ with Ala and replacement of $R221\&236_{LGN}$ with Ala lead to the complete disruption of the LGN/Fmpd1 complex formation. A significant decrease in LGN/NuMA binding was observed when $E922_{Frmpd1}$, $E929_{Frmpd1}$, $K931_{Frmpd1}$, or $K96\&R135_{LGN}$ was substituted with Ala (Fig. 3c and d). Noted that the above-selected mutation sites in LGN, especially for the R221 site, play a pivotal role for high-affinity binding between LGN/Pins and its targets mInsc/

Insc, or NuMA.[12–14] Importantly, amino acid sequence alignment analysis reveals that most of the key residues involved in the LGN/Frmpd1 interaction are evolutionary conserved, indicating that the LGN/Frmpd1 interaction mode observed here can be extended to corresponding interactions in other species (Fig. 1b and Ref. 12).

Comparison with the known LGN/Pins TPR/target complex structures

To find out the target recognition mode of LGN-TPR, we compared the structures of the LGN/Frmpd1, LGN/NuMA, LGN/mInsc, and its *Drosophila* counterpart Pins/Insc complexes. The conformations

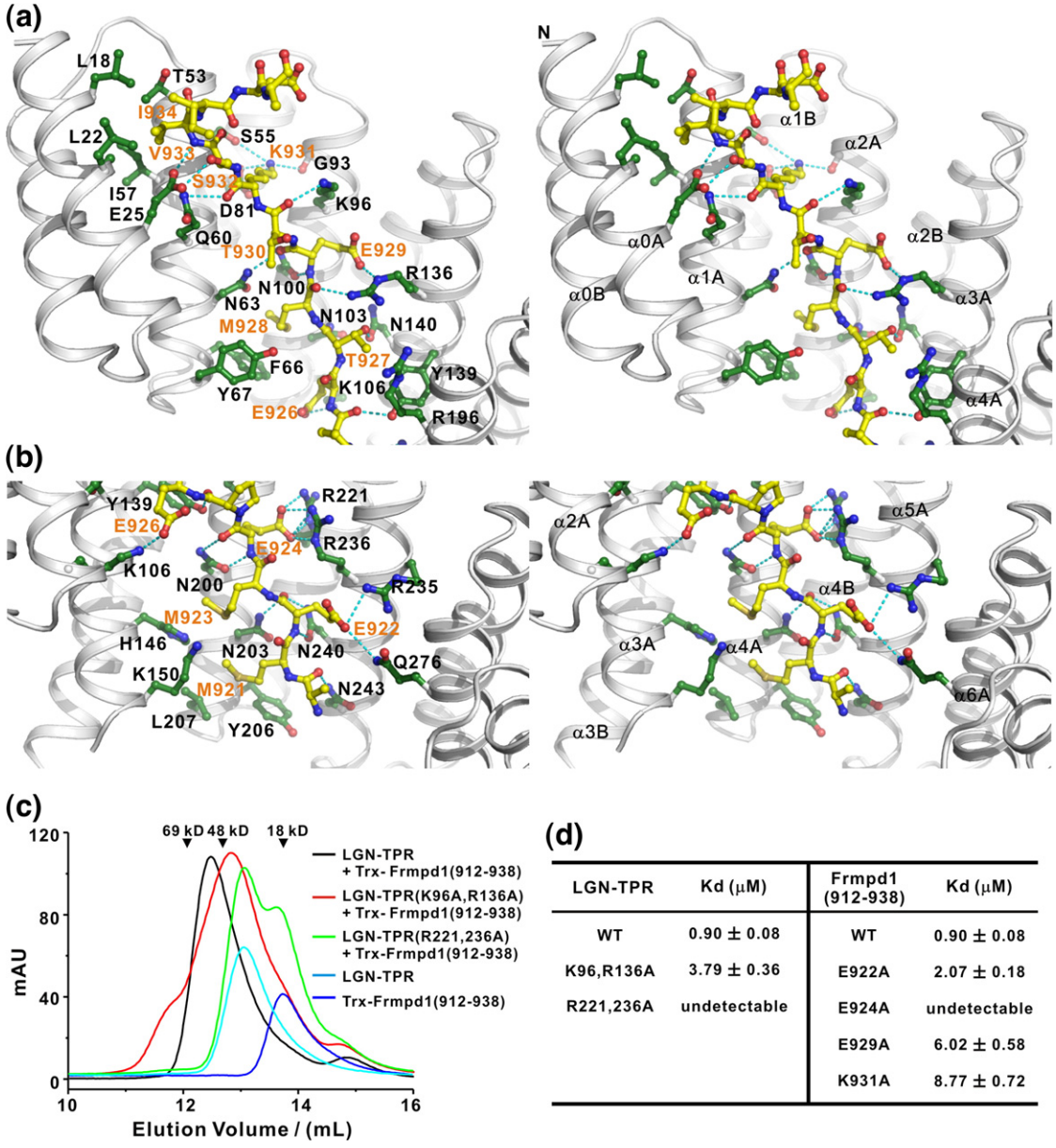

(d)

LGN-TPR	Kd (μM)	Frmpd1 (912-938)	Kd (μM)
WT	0.90 ± 0.08	WT	0.90 ± 0.08
K96,R136A	3.79 ± 0.36	E922A	2.07 ± 0.18
R221,236A	undetectable	E924A	undetectable
		E929A	6.02 ± 0.58
		K931A	8.77 ± 0.72

Fig. 3. The interaction interface of the LGN/Frmpd1 complex. The LGN/Frmpd1 interface is divided into two parts corresponding to LGN-TPR0-3/Frmpd1_C (a) and LGN-TPR4-7/Frmpd1_N (b). The interaction details between LGN and Frmpd1 in the two parts are shown in stereoview. The side chains of the residues involved in the interdomain interactions are drawn in stick model. Charge–charge and hydrogen bonding interactions are highlighted by broken lines in cyan. (c) Analytical gel-filtration analysis showing the bindings of LGN-TPR and its mutants with Trx-Frmpd1(912–938). The elution volumes of the molecular mass standards are indicated at the top of the panel. (d) Summary of the bindings of LGN-TPR and its selected mutants to various Frmpd1(912–938) fragments derived from the ITC-based measurements.

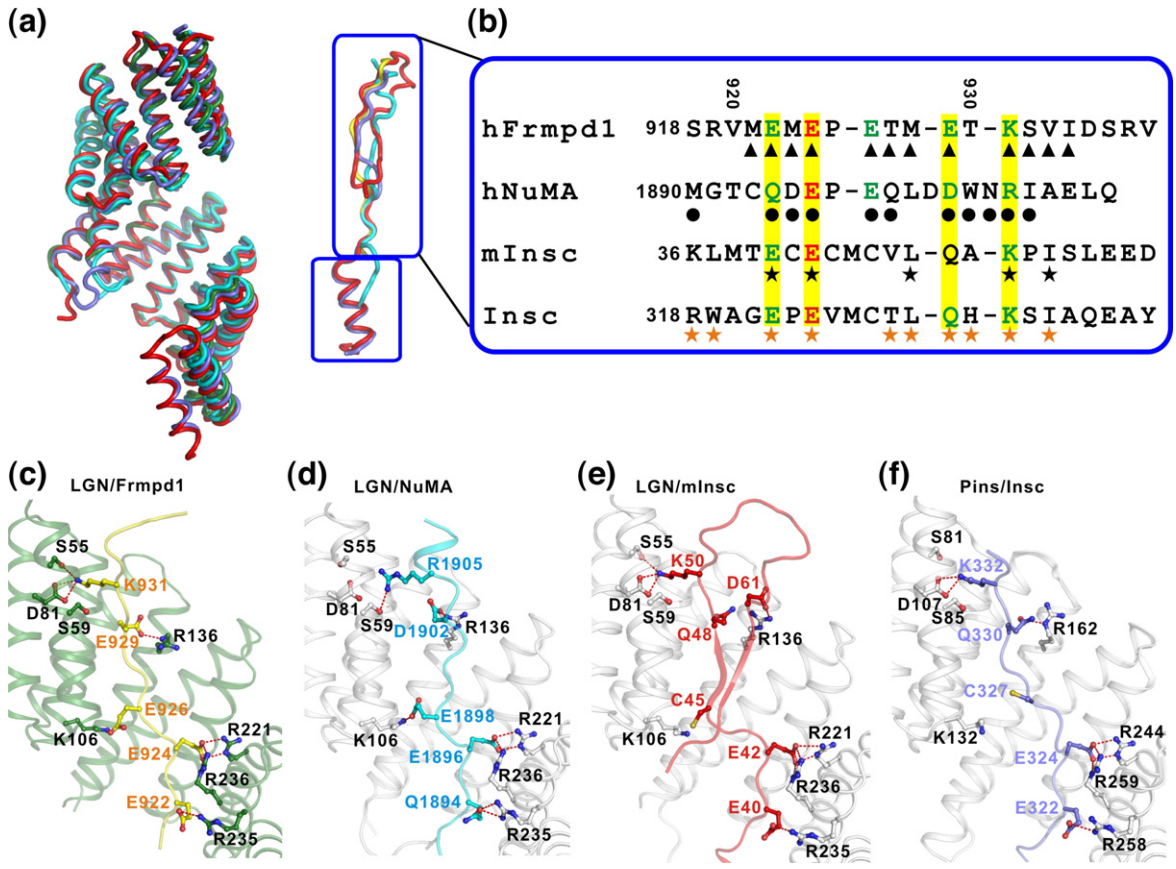

Fig. 4. Comparison of the LGN/Frmpd1, LGN/NuMA, LGN/mInsc, and Pins/Insc complex structures. (a) Worm diagram representation showing the superposition of the TPR and fragments, respectively, from the LGN (green)/Frmpd1 (yellow), LGN (cyan)/NuMA (cyan) (PDB ID: 3RO2), LGN (red)/mInsc (red) (PDB ID: 3SF4), and Pins (blue)/Insc (blue) (PDB ID: 4A1S) complexes. (b) Structure-based sequence alignment of the LGN/Pins TPR-binding fragments from Frmpd1, NuMA, mInsc, and Insc revealing the conserved "E/QxEx$_{4\text{-}5}$E/D/Qx$_{1\text{-}2}$K/R" sequence highlighted in yellow. In the alignment, the absolutely conserved amino acids are highlighted in red, and the highly conserved residues are in green. The residues responsible for TPR binding are indicated with triangles in Frmpd1, circle in NuMA, black pentacle in mInsc, and orange pentacle in Insc. (c–f) Comparison of the LGN/Frmpd1 (c), LGN/NuMA (d), LGN/mInsc (e), and Pins/Insc (f) interaction interfaces. A selected set of amino acid residues, which are in the interdomain interfaces and share similar positions in these complexes, are drawn in the stick model. For clearance, the residues 15–49 in LGN and residues 41–75 in Pins are removed from the figure.

of TPRs in the four complexes are highly similar, and the binding sites of the four TPR-binding fragments on LGN/Pins TPRs are partially overlapped (Fig. 4a). All the fragments run antiparallel to LGN/Pins TPRs and align well with the axis of the TPR superhelix. Of the four LGN/Pins TPR-binding fragments, both mInsc and Insc contain an N-terminal α-helix that extensively interacts with TPR5-7 of LGN/Pins.[12,14] Importantly, this N-terminal α-helix and TPR5-7 interaction accounts for the majority of the binding energy between mInsc and LGN.[12,14] The mInsc(Insc)/TPR interaction is further strengthened by the packing between the C-terminal part of the mInsc/Insc fragment and TPR0-5. This C-terminal extension of mInsc is missing in our previous mInsc/LGN complex structure.[12] It is noted that residues in the β2 strand of the mInsc fragment are not conserved in Insc, and the corresponding α–loop–β1 region in Insc is sufficient for binding to Pins TPR with high affinity.[13] Thus, the β1–loop–β2 module might only exist in mInsc rather than its *Drosophila* homologue. The NuMA and Frmpd1 fragments, as well as the C-terminal part of the Insc fragments, form extended structures and contact with TPR0-5 through numerous charge–charge interactions as well as a few hydrophobic interactions (Fig. 3a and b).[12,13]

A close-up view of the interfaces of the four complexes reveals that several charge–charge interaction pairs are highly conserved. For example, the Arg235$_{LGN}$–Glu922$_{Frmpd1}$ and Arg221, Arg236$_{LGN}$–Glu924$_{Frmpd1}$ salt bridges are conserved in all the four complexes, although the Glu922$_{Frmpd1}$ is replaced by Gln1894$_{NuMA}$ in the LGN/NuMA complex (Fig. 4c–f). In addition, the Arg221,

$Arg236_{LGN}$–$Glu924_{Frmpd1}$ salt bridge is critical for high-affinity complex formation between LGN/Pins TPRs and its targets (Fig. 3c and d).[12–14] Based on the structure comparison of the four complexes, a new structure-based sequence alignment of the four LGN-TPR-binding fragments has been made (Fig. 4b), indicating a consensus "E/Q-x-E" triad as a core binding motif. The backbone conformations of the four fragments at this consensus "E/Q-x-E" triad are also highly similar (Fig. 4a). The salt bridge of $Arg136_{LGN}$–$Glu929_{Frmpd1}$ in a way is conserved in all the four complexes: the $Glu929_{Frmpd1}$ is replaced by $Asp1902_{NuMA}$ and $Gln330_{Insc}$ in the LGN/NuMA and Pins/Insc complexes, respectively; in the LGN/mInsc complex, the $Arg136_{LGN}$ forms salt bridge with $Asp61_{mInsc}$ from β2 instead of $Gln48_{mInsc}$ (corresponding to $Gln330_{Insc}$) from β1. These interactions have been shown to strengthen the LGN/Frmpd1 or

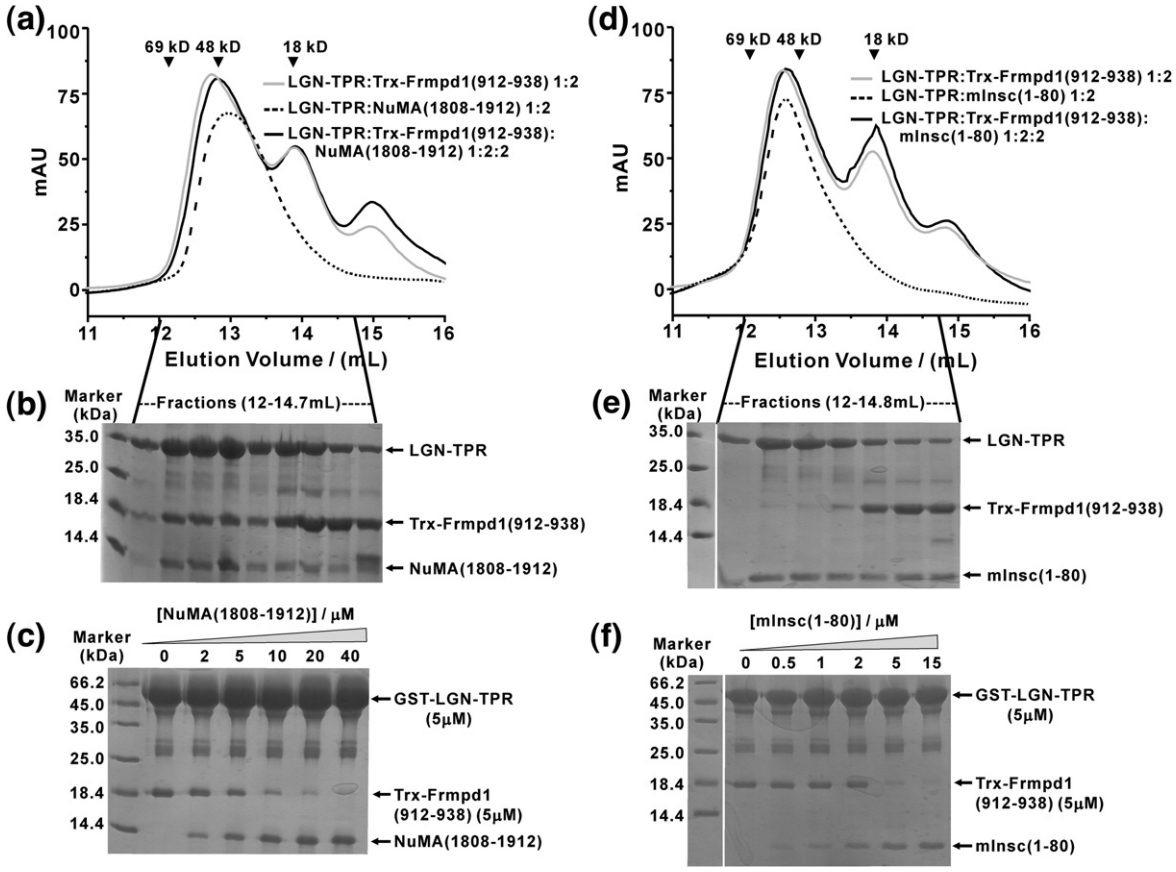

Fig. 5. Characterization of the interaction of Frmpd1, NuMA, and mInsc with LGN. (a) Analytical gel-filtration elution profile of the LGN-TPR/Trx-Frmpd1(912–938)/NuMA(1808–1912) mixture at a 1:2:2 molar ratio. For comparison, the elution profiles of LGN-TPR/Trx-Frmpd1(901–938) and LGN-TPR/NuMA(1808–1912) mixtures each at a 1:2 molar ratio are also shown. The elution volumes of the molecular size markers are indicated by arrowheads at the top. (b) SDS-PAGE analysis of the protein components of the eluted peak of the LGN-TPR/Trx-Frmpd1(912–938)/NuMA(1808–1912) mixture in (a). The elution peak was collected with 0.3 ml/fraction, and nine fractions corresponding to the elution volumes from 12 to 14.7 ml were analyzed by SDS-PAGE. (c) Sub-stoichiometric amounts of Frmpd1 and NuMA can compete with each other for binding to LGN. In this experiment, the amounts of GST-LGN-TPR and Trx-Frmpd1 in each assay were fixed at 5 μM, and the concentrations of NuMA were gradually increased. The formations of the LGN/Frmpd1 and LGN/NuMA complexes were assayed using the GSH-coupled Sepharose beads pull-down assay. (d) Analytical gel-filtration elution profile of the LGN-TPR/Trx-Frmpd1(912–938)/mInsc(1–80) mixture at a 1:2:2 molar ratio. For comparison, the elution profiles of LGN-TPR/Trx-Frmpd1(912–938) and LGN-TPR/mInsc(1–80) mixture each at a 1:2 molar ratio are also shown. The elution volumes of the molecular size markers are indicated by arrowheads at the top. (e) SDS-PAGE analysis of the protein components of the eluted peak of the LGN-TPR/Trx-Frmpd1(912–938)/mInsc(1–80) mixture in (d). The elution peak was collected with 0.4 ml/fraction, and seven fractions corresponding to the elution volumes from 12 to 14.8 ml were analyzed by SDS-PAGE. (f) Dose-dependent binding competition experiment showing that mInsc dominates over Frmpd1 in binding to LGN-TPR. In this experiment, the total amounts of GST-LGN-TPR and Trx-Frmpd1 were fixed (5 μM), and the concentrations of mInsc were gradually increased. The same GSH-Sepharose beads pull-down experiment was used to assay the formations of the LGN/Frmpd1 or LGN/mInsc complexes.

LGN/NuMA packing (Fig. 3c and d).[12] Another conserved TPR/target packing force is the Ser55, $Asp81_{LGN}$–$Lys931_{Frmpd1}$ hydrogen bonds that are also present in the LGN/mInsc and Pins/Insc complexes; in LGN/NuMA complex, the $R1905_{NuMA}$ (corresponding to $Lys931_{Frmpd1}$) makes hydrogen bond with $Ser59_{LGN}$ instead of $Ser55_{LGN}$. Furthermore, the salt bridge of $Lys106_{LGN}$–$Glu926_{Frmpd1}$ contributing to TPR/target binding is also present in the LGN/NuMA complex, but neither in LGN/mInsc nor in Pins/Insc (Fig. 4c–f). Interestingly, the backbone conformation of NuMA fragment deviates from the other three at $Leu1900_{NuMA}$ and more or less overlaps with the β2 strand of mInsc (Fig. 4a). Although NuMA has the similar key residues for TPR binding C-terminal to Leu1900 (e.g., D1902 and R1905), the NuMA sequence at this region is longer than the other three proteins (Fig. 4b). This may result in the different backbone conformation of NuMA. Overall, based on the above structural and sequence analysis of these four complexes, an extended consensus sequence motif of LGN/Pins TPR binding targets can be summarized as "E/QxEx$_{4-5}$E/D/Qx$_{1-2}$K/R", where x denotes any amino acids (Fig. 4b).

Comparisons of the bindings of Frmpd1, NuMA, and mInsc to LGN-TPRs

To examine whether Frmpd1 can bind to LGN in the presence of NuMA or mInsc, we characterized the LGN/Frmpd1 complex formation with and without the presence of NuMA or mInsc using the analytical gel-filtration and pull-down-based competition assays. When LGN-TPR was incubated with both Frmpd1 and NuMA at a 1:2:2 molar ratio, analytical gel-filtration analysis showed that the mixture had an elution volume between those of the TPR/Frmpd1 and TPR/NuMA complexes, indicating the presence of a mixture of both TPR/Frmpd1 and TPR/NuMA complexes in the solution (Fig. 5a). The SDS-PAGE analysis of the elution peak for the LGN-TPR/Frmpd1/NuMA mixture confirmed the above conclusion (Fig. 5b). *In vitro* competition experiments further showed that addition of increasing amounts of NuMA can effectively compete with Frmpd1 for binding to LGN (Fig. 5c), consistent with the fact that Frmpd1 and NuMA binds to LGN in a highly similar mode (Fig. 4c and d and Ref. 12).

As mInsc has been shown to have a priority over NuMA in binding to LGN, we next tested whether mInsc can also displace Frmpd1 from LGN. When LGN-TPR was incubated with both mInsc and Frmpd1 at a 1:2:2 molar ratio, no detectable ternary complex was formed (Fig. 5d and e). Competition experiments further showed that 1:1 stoichiometric amount of mInsc can effectively displace Frmpd1 from LGN (Fig. 5f). This result indicates that the interaction between Frmpd1 and LGN can also be disrupted by mInsc as that between NuMA and LGN.[12] This can be rationalized by the crystal structures of LGN/Pins in complex with various targets, in which Insc/mInsc contain a high-affinity LGN-TPR5-7 binding α-helix in addition to the extension sequence binding to LGN TRP0-5 common for all the LGN-TPR binding partners known so far.

Discussion

In asymmetric cell division, LGN/Pins plays an essential role in orienting the mitotic spindle along the axis of cell polarity, and the functions of LGN/Pins are executed mainly by its protein–protein interacting modules, the N-terminal TPR motifs, and the C-terminal GoLoco motifs. Each of the GoLoco motifs from LGN/Pins is capable to bind to GDP-bound Gαi for cortical localization of the protein, and both LGN and Pins have diverse TPR binding partners that influence their subcellular location in cell division (i.e., LGN/NuMA,[12,18,22] Pins/Mud,[8,9] LGN/mInsc,[12,27] Pins/Insc,[6,17] and LGN/Lgl2[28]). The LGN/Frmpd1 interaction characterized in this work is another example of TPR-motif-mediated target recognition. Frmpd1 binds to LGN-TPR with a similar mode as NuMA does. Although the functions of Frmpd1 have not been well defined, it is recently reported as a regulatory binding partner of AGS3 and influences its subcellular location.[26] Frmpd1 interacts with the TPR motifs of AGS3 and thus stabilizes the population of the protein in the membrane fraction. Taking into account of the high similarity of the TPR motifs from LGN and AGS3 (77% sequence identity), the LGN/Frmpd1 interaction characterized in this work might provide another molecular mechanism in regulating the subcellular positioning of LGN.

Together with the recently reported LGN/mInsc, LGN/NuMA, and Pins/Insc complex structures, the LGN/Frmpd1 complex structure solved in this work is the fourth case of LGN/Pins TPR/target interaction. These four complex structures reveal the target recognition specificity and versatility of LGN/Pins TPRs. The tandem array of eight TPR motifs forms a versatile platform for target binding. The four complexes show two distinct regions of target binding in the LGN/Pins TPR motifs: TPR5-7 uniquely recognizes the N-terminal α-helix of mInsc/Insc, and TPR0-5 binds the extended structures of NuMA, mInsc, Insc, and Frmpd1 with a similar binding mode. The binding of mInsc/Insc fragment covers both regions of TPR motifs and can be viewed as a typical two-site binding. The LGN/NuMA and LGN/Frmpd1 interaction, however, only involves the second target recognition region of TPR0-5. These structures also allow us to obtain a more accurate sequence alignment of the TPR

binding partners, giving a consensus TPR0-5 recognition sequence of "E/QxEx$_{4-5}$E/D/Qx$_{1-2}$K/R". It is worth noting that LGN/Pins TPRs are flexibly designed to recognize this sequence motif. For example, NuMA has more intervening residues than the other three fragments and adopts slightly different backbone conformation, while mInsc uses the β2 strand to complement the TPR interactions. Therefore, we can envision that the TPR motifs of LGN/Pins serve as a versatile platform for protein–protein interaction that can recognize a wide spectrum of binding partners. These two binding modes distinguish mInsc/Insc from Frmpd1 and NuMA in binding to LGN-TPRs, and as shown in the competition experiments, mInsc can effectively disrupt the binding of NuMA or Frmpd1 to LGN.[12,14] Although the LGN/Pins binding partner that targets only the TPR5-7 binding site has not been discovered so far, it is reasonable to speculate that proteins with similar sequence motif as the N-terminal α-helix of Insc/mInsc are potential binding partners of LGN/Pins.

Materials and Methods

Protein expression and purification

The human Frmpd1 fragments [Frmpd1(901–938), Frmpd1(912–938), and Frmpd1(939–951)], the mouse LGN-TPR motifs (LGN-TPR, amino acids 15–350), the mouse Insc N-terminal fragment [mInsc(1–80)], and the human NuMA C-terminal fragment [NuMA(1808–1912)] were individually cloned into a modified version of pET32a vector. The resulting proteins each contained a Trx tag in their N termini. All the mutations used in this study were created using the standard PCR-based mutagenesis method and confirmed by DNA sequencing. Recombinant proteins were expressed in *Escherichia coli* BL21 (DE3) host cells at 16 °C and were purified by using a Ni^{2+}-NTA agarose affinity chromatography followed by size-exclusion chromatography. The N-terminal Trx-tagged fragments of LGN-TPR were cleaved by digesting the fusion protein with protease 3C, and the proteins were purified by another step of size-exclusion chromatography. For crystallization, freshly purified Trx-tagged LGN-TPR and Trx-tagged Frmpd1(912–938) were mixed at a 1:2 molar ratio, and the complex was purified using size-exclusion chromatography. The N-terminal Trx-tagged fragments were then cleaved by digesting the fusion protein complex with 3C protease, and the LGN/Frmpd1 complex was purified by another step of size-exclusion chromatography. For *in vitro* biochemical analysis, the LGN-TPR were expressed as the GST-fused protein and purified by GSH-Sepharose affinity chromatography.

Crystallography

Crystals of LGN/Frmpd1 complex were obtained by the hanging-drop vapor diffusion method at 18 °C. Freshly purified LGN/Frmpd1 complex was concentrated to 0.5 mM and then set up in hanging drop with equal volumes of 0.2 M NaCl, 0.1 M 2-[bis(2-hydroxyethyl) amino]-2-(hydroxymethyl)propane-1,3-diol (pH 6.5), and 25% w/v polyethylene glycol 3350. The diffraction data of crystals were collected at Shanghai Synchrotron Radiation Facility (SSRF) BL17U. The phase problem was solved by molecular replacement using the LGN/NuMA structure [PDB (*P*rotein *D*ata *B*ank) ID: 3RO2] as the search model with Phaser[29] against the 2.4-Å resolution data set. Then, anisotropic refinement was applied using SHELXL.[30] Further manual model building and adjustment were completed using Coot.[31] The final refinement statistics are summarized in Table 1.

ITC measurements

ITC measurements were performed on an ITC200 microcalorimeter (MicroCal) at 18 °C. All protein samples were dissolved in a buffer containing 50 mM Tris (pH 8.0), 100 mM NaCl, and 1 mM ethylenediaminetetraacetic acid (EDTA). The titration was carried out by injecting 40-μl aliquots of various Trx-Frmpd1 fragments (0.35 mM) into LGN-TPR (0.04 mM) at time intervals of 2 min to ensure that the titration peak returned to the baseline. The titration data were analyzed using the program Origin7.0 and fitted by the one-site binding model.

GST pull-down assay

For GST pull-down assay, GST or GST-tagged proteins (3 μM for the final concentration) were first loaded to 50-μl GSH-Sepharose 4B slurry beads in a 500-μl assay buffer containing 50 mM Tris (pH 8.0), 100 mM NaCl, 1 mM DTT, and 1 mM EDTA. The GST fusion protein loaded beads were then mixed with potential binding partners (6 μM for the final concentration), and the mixtures were incubated for 2 h at 4 °C. After three times washing, the proteins captured by affinity beads were eluted by boiling, resolved by 15% SDS-PAGE, and detected by Coomassie blue staining.

Analytical gel-filtration chromatography

Analytical gel-filtration chromatography was carried out on an AKTA FPLC system (GE Healthcare). Proteins were loaded onto a Superose 12 10/300 GL column 20 (GE Healthcare) equilibrated with a buffer containing 50 mM Tris (pH 8.0), 100 mM NaCl, 1 mM DTT, and 1 mM EDTA. The loading concentration of LGN-TPR was fixed at 15 μM, and the concentrations of other proteins were specifically indicated.

Accession number

The atomic coordinates of LGN/Frmpd1 complex have been deposited in the PDB with accession number 4G2V.

Acknowledgements

We thank the SSRF BL17U for X-ray beam time. This work was supported by the National

Major Basic Research Program (2009CB918600 and 2011CB808505), National Science Foundation of China (30970574, 31270778, 20973040, and 31070642), the Shanghai Rising-Star Program (10QA1400700), and Science and Technology Commission of Shanghai Municipality (08DZ2270500) to W. Wang and W. Wen and by grants 663610, 663811, HKUST6/CRF/10, and AoE/M-04/04 from the Research Grants Council of Hong Kong to M.Z.

Supplementary Data

Supplementary data to this article can be found online at http://dx.doi.org/10.1016/j.jmb.2013.01.003

Received 13 July 2012;
Received in revised form 28 December 2012;
Accepted 7 January 2013
Available online 11 January 2013

Keywords:
asymmetric cell division;
LGN;
TPR motif;
Frmpd1

Abbreviations used:
TPR, tetratricopeptide repeat; Frmpd1, FERM and PDZ domain containing 1; GST, glutathione *S*-transferase; ITC, isothermal titration calorimetry; SSRF, Shanghai Synchrotron Radiation Facility; EDTA, ethylenediaminetetraacetic acid.

References

1. Morrison, S. J. & Kimble, J. (2006). Asymmetric and symmetric stem-cell divisions in development and cancer. *Nature*, **441**, 1068–1074.
2. Cowan, C. R. & Hyman, A. A. (2004). Asymmetric cell division in *C. elegans*: cortical polarity and spindle positioning. *Annu. Rev. Cell Dev. Biol.* **20**, 427–453.
3. Siller, K. H. & Doe, C. Q. (2009). Spindle orientation during asymmetric cell division. *Nat. Cell Biol.* **11**, 365–374.
4. Knoblich, J. A. (2008). Mechanisms of asymmetric stem cell division. *Cell*, **132**, 583–597.
5. Gonczy, P. (2008). Mechanisms of asymmetric cell division: flies and worms pave the way. *Nat. Rev., Mol. Cell Biol.* **9**, 355–366.
6. Yu, F., Morin, X., Cai, Y., Yang, X. & Chia, W. (2000). Analysis of partner of inscuteable, a novel player of *Drosophila* asymmetric divisions, reveals two distinct steps in inscuteable apical localization. *Cell*, **100**, 399–409.
7. Parmentier, M. L., Woods, D., Greig, S., Phan, P. G., Radovic, A., Bryant, P. & O'Kane, C. J. (2000). Rapsynoid/partner of inscuteable controls asymmetric division of larval neuroblasts in *Drosophila*. *J. Neurosci.* **20**, RC84.
8. Siller, K. H., Cabernard, C. & Doe, C. Q. (2006). The NuMA-related Mud protein binds Pins and regulates spindle orientation in *Drosophila* neuroblasts. *Nat. Cell Biol.* **8**, 594–600.
9. Izumi, Y., Ohta, N., Hisata, K., Raabe, T. & Matsuzaki, F. (2006). *Drosophila* Pins-binding protein Mud regulates spindle-polarity coupling and centrosome organization. *Nat. Cell Biol.* **8**, 586–593.
10. Bowman, S. K., Neumuller, R. A., Novatchkova, M., Du, Q. & Knoblich, J. A. (2006). The *Drosophila* NuMA homolog Mud regulates spindle orientation in asymmetric cell division. *Dev. Cell*, **10**, 731–742.
11. Schuyler, S. C. & Pellman, D. (2001). Search, capture and signal: games microtubules and centrosomes play. *J. Cell Sci.* **114**, 247–255.
12. Zhu, J., Wen, W., Zheng, Z., Shang, Y., Wei, Z., Xiao, Z. *et al.* (2011). LGN/mInsc and LGN/NuMA complex structures suggest distinct functions in asymmetric cell division for the Par3/mInsc/LGN and Gαi/LGN/NuMA pathways. *Mol. Cell*, **43**, 418–431.
13. Culurgioni, S., Alfieri, A., Pendolino, V., Laddomada, F. & Mapelli, M. (2011). Inscuteable and NuMA proteins bind competitively to Leu-Gly-Asn repeat-enriched protein (LGN) during asymmetric cell divisions. *Proc. Natl Acad. Sci. USA*, **108**, 20998–21003.
14. Yuzawa, S., Kamakura, S., Iwakiri, Y., Hayase, J. & Sumimoto, H. (2011). Structural basis for interaction between the conserved cell polarity proteins Inscuteable and Leu-Gly-Asn repeat-enriched protein (LGN). *Proc. Natl Acad. Sci. USA*, **108**, 19210–19215.
15. Willard, F. S., Kimple, R. J. & Siderovski, D. P. (2004). Return of the GDI: the GoLoco motif in cell division. *Annu. Rev. Biochem.* **73**, 925–951.
16. Blatch, G. L. & Lassle, M. (1999). The tetratricopeptide repeat: a structural motif mediating protein–protein interactions. *BioEssays*, **21**, 932–939.
17. Schaefer, M., Shevchenko, A., Shevchenko, A. & Knoblich, J. A. (2000). A protein complex containing Inscuteable and the Gα-binding protein Pins orients asymmetric cell divisions in *Drosophila*. *Curr. Biol.* **10**, 353–362.
18. Du, Q. & Macara, I. G. (2004). Mammalian Pins is a conformational switch that links NuMA to heterotrimeric G proteins. *Cell*, **119**, 503–516.
19. Yu, F., Cai, Y., Kaushik, R., Yang, X. & Chia, W. (2003). Distinct roles of Gαi and Gβ13F subunits of the heterotrimeric G protein complex in the mediation of *Drosophila* neuroblast asymmetric divisions. *J. Cell Biol.* **162**, 623–633.
20. Yu, F., Morin, X., Kaushik, R., Bahri, S., Yang, X. & Chia, W. (2003). A mouse homologue of *Drosophila* pins can asymmetrically localize and substitute for pins function in *Drosophila* neuroblasts. *J. Cell Sci.* **116**, 887–896.
21. Izaki, T., Kamakura, S., Kohjima, M. & Sumimoto, H. (2006). Two forms of human Inscuteable-related protein that links Par3 to the Pins homologues LGN and AGS3. *Biochem. Biophys. Res. Commun.* **341**, 1001–1006.
22. Du, Q., Stukenberg, P. T. & Macara, I. G. (2001). A mammalian partner of inscuteable binds NuMA and regulates mitotic spindle organization. *Nat. Cell Biol.* **3**, 1069–1075.

23. D'Andrea, L. D. & Regan, L. (2003). TPR proteins: the versatile helix. *Trends Biochem. Sci.* **28**, 655–662.
24. Kumar, A., Roach, C., Hirsh, I. S., Turley, S., deWalque, S., Michels, P. A. & Hol, W. G. (2001). An unexpected extended conformation for the third TPR motif of the peroxin PEX5 from *Trypanosoma brucei*. *J. Mol. Biol.* **307**, 271–282.
25. Das, A. K., Cohen, P. W. & Barford, D. (1998). The structure of the tetratricopeptide repeats of protein phosphatase 5: implications for TPR-mediated protein–protein interactions. *EMBO J.* **17**, 1192–1199.
26. An, N., Blumer, J. B., Bernard, M. L. & Lanier, S. M. (2008). The PDZ and band 4.1 containing protein Frmpd1 regulates the subcellular location of activator of G-protein signaling 3 and its interaction with G-proteins. *J. Biol. Chem.* **283**, 24718–24728.
27. Zigman, M., Cayouette, M., Charalambous, C., Schleiffer, A., Hoeller, O., Dunican, D. *et al.* (2005). Mammalian inscuteable regulates spindle orientation and cell fate in the developing retina. *Neuron*, **48**, 539–545.
28. Yasumi, M., Sakisaka, T., Hoshino, T., Kimura, T., Sakamoto, Y., Yamanaka, T. *et al.* (2005). Direct binding of Lgl2 to LGN during mitosis and its requirement for normal cell division. *J. Biol. Chem.* **280**, 6761–6765.
29. McCoy, A. J., Grosse-Kunstleve, R. W., Adams, P. D., Winn, M. D., Storoni, L. C. & Read, R. J. (2007). Phaser crystallographic software. *J. Appl. Crystallogr.* **40**, 658–674.
30. Sheldrick, G. M. (2008). A short history of SHELX. *Acta Crystallogr., Sect. A: Found. Crystallogr.* **64**, 112–122.
31. Emsley, P. & Cowtan, K. (2004). Coot: model-building tools for molecular graphics. *Acta Crystallogr., Sect. D: Biol. Crystallogr.* **60**, 2126–2132.